Rare Metal Materials and Engineering
Volume 55, Issue 2, February 2026
Available online at www.rmme.ac.cn

Science Press

Cite this article as: Wang Yumiao, Liang Wenjun, Li Xiaoli, et al. Influence of Homogenization on Microstructure Characteristics of Yttrium-Modified GH3535 Alloy[J]. Rare Metal Materials and Engineering, 2026, 55(02): 322-332. DOI: https://doi.org/10.12442/j.issn.1002-185X.20250038.

ARTICLE

Influence of Homogenization on Microstructure Characteristics of Yttrium-Modified GH3535 Alloy

Wang Yumiao[1,2], Liang Wenjun[2,3], Li Xiaoli[2], Jiang Sheng[4], Zhou Xingtai[2], Qiu Hanxun[1]

[1] School of Materials and Chemistry, University of Shanghai for Science and Technology, Shanghai 200093, China; [2] Shanghai Institute of Applied Physics, Chinese Academy of Sciences, Shanghai 201800, China; [3] School of Nuclear Science and Technology, University of Chinese Academy of Sciences, Beijing 100049, China; [4] Shanghai Advanced Research Institute, Chinese Academy of Sciences, Shanghai 201210, China

Abstract: The influence of homogenization parameters on element segregation, dendritic structure, and the precipitate evolution in the GH3535-0.08wt% Y alloy was investigated. Additionally, some specific homogenization parameters were maintained constant throughout the experiments. Results indicate that the heat treatment at 1150 °C for 10 h is the optimal homogenization condition. Following this optimal treatment, dendrite structures and element segregation are eliminated. Furthermore, both SiC and Y_5Si_3 precipitates in the as-cast alloy decrease significantly. Conversely, the homogenization at 1188 °C induces overheating defects within the alloy. Although SiC and Y_5Si_3 phases also decrease, some large M_6C phases can still be observed, adversely affecting subsequent forging processes.

Key words: Ni-based alloy; Y; microstructure; homogenization; carbide

1 Introduction

Traditional energy sources, such as oil and coal, contribute significantly to environmental pollution. The emerging issues related to energy and environment are gradually receiving increased attention. Nuclear power, recognized for its cleanliness and efficiency, has also garnered substantial interest. Molten salt reactor (MSR), which uses molten salts as coolants, is classified as a fourth-generation reactor with excellent safety performance and unique advantages, including high temperature operation at low pressure[1–2]. During MSR operations, structural materials must directly interact with the high-temperature molten salt coolant. Thus, these materials require excellent high-temperature strength and outstanding resistance to molten salt corrosion. GH3535 alloy, a nickel-based superalloy with excellent performance at 650–700 °C, is usually employed as the structural material for MSRs[3]. However, because MSRs are anticipated to operate above 700 °C, GH3535 alloy does not fulfill this requirement. Numerous studies indicate that doping trace amount of rare-earth elements (REEs) in superalloys can significantly enhances their performance. However, excessive REE content may yield adverse effects[4–6]. For GH3535 alloy, it is demonstrated that the incorporation of trace amount of REE yttrium (Y) can significantly enhance the high-temperature strength, resistance against tellurium brittleness, and corrosion resistance of alloys[7–10]. Besides, GH3535 alloy has a mature heat treatment process. However, both the optimal Y addition content and subsequent heat treatment processes for GH3535-Y alloy are not optimized, particularly concerning the control over trace REE addition into the solid solution. In addition, most researches are based on the button ingot, which makes it difficult to add extremely accurate and tiny amount of yttrium. To ensure that the final workpiece of GH3535-Y alloy can be applied to the structural material of MSRs in the future, it is necessary to clarify the alloy melting and heat treatment

Received date: February 17, 2025
Foundation item: National Natural Science Foundation of China (51801227, 52071331)
Corresponding author: Li Xiaoli, Ph. D., Associate Researcher, Shanghai Institute of Applied Physics, Chinese Academy of Sciences, Shanghai 201800, P. R. China, E-mail: lixiaoli@sinap.ac.cn; Zhou Xingtai, Ph. D., Associate Researcher, Shanghai Institute of Applied Physics, Chinese Academy of Sciences, Shanghai 201800, P. R. China, E-mail: zhouxingtai@sinap.ac.cn; Qiu Hanxun, Ph. D., Associate Professor, School of Materials and Chemistry, University of Shanghai for Science and Technology, Shanghai 200093, P. R. China, E-mail: hxqiu@usst.edu.cn

processes of the alloy. During the solidification process, when undercooling occurs, nucleation and growth processes for solid grains are inhibited, leading to dendrites as predominant structures during primary solidification. Dendritic growth arises from multiple initiation points within the molten alloy during solidification, leading to the branching structure of dendrites[11–13]. This dendritic formation is accompanied by the significant segregation, which can influence critical alloy properties, such as machinability, strength, ductility, and corrosion resistance. Consequently, it is imperative to eliminate the dendrite structure through homogenization to achieve a uniform element distribution[14–15]. For the GH3535-Y alloy, segregation of Y and other elements occurs within the matrix, leading to the formation of detrimental intermetallic compounds (Ni-Y), which adversely affect Y concentration in solid solution as well as overall properties of GH3535-Y alloy[9,16]. The heat treatment process influences element distribution among alloy constituents and precipitated phases, ultimately impacting alloy performance. Homogenization serves as a crucial heat treatment step, aiming at minimizing or even eliminating element segregation while reducing cracking during forging processes[15]. Therefore, it is essential to investigate the Y distribution within GH3535-Y alloys alongside its influence on microstructure throughout homogenization.

In this research, the alloy ingots of 20 kg were used to investigate the homogenization conditions for GH3535 alloy with Y addition and to analyze the microstructure evolution of the alloy during the homogenization process. Differential thermal analysis (DTA) was performed to ascertain the phase transition temperatures of the alloy and to identify the homogenization temperature parameters. Furthermore, the effects of the homogenization conditions on the microstructure of GH3535 alloy with Y addition were investigated. This research provides optimal homogenization conditions for large-scale alloy ingots (tens of kilograms), thereby laying a robust foundation for subsequent forging processes.

2 Experiment

The chemical composition of the Y-containing GH3535 alloy ingot used in this experiment is shown in Table 1. The appearance of the alloy ingot before homogenization is depicted in Fig. 1. The ingot from outer to inner side is composed of a fine-grain zone, a columnar crystal zone with columnar grains, and a central equiaxed zone. Subsequently, the ingots underwent the homogenization treatment under different conditions (1150 °C for 2, 5, and 10 h; 1188 °C for 2, 5, and 10 h), followed by a slow cooling after the insulation stage. Small samples of 2 mm×10 mm×20 mm were extracted from the ingot after the homogenization for characterization.

Table 1 Chemical composition of GH3535-Y alloy (wt%)

Y	Cr	Fe	Mo	Si	Mn	Ni
0.08	6.91	0.01	16.45	0.35	0.67	Bal.

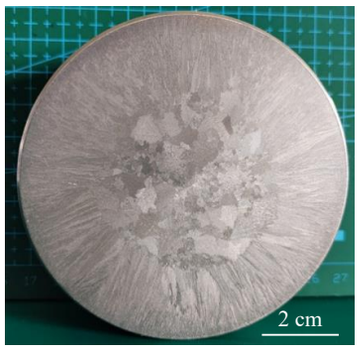

Fig.1 Appearance of GH3535-Y alloy ingot before homogenization

All samples were ground with SiC sandpaper (800#–3000#) and then polished with Al_2O_3 polishing solution. The defects and carbide distribution of ground samples were observed by optical microscope (OM). Then, the samples were etched by aqua regia (hydrochloric acid: nitric acid=3:1) to observe the crystal phase structure. The microstructure of the alloy was analyzed using OM, scanning electron microscope (SEM), and electron probe X-ray microanalyzer (EPMA). The element distribution and precipitated phases were analyzed by energy dispersive spectrometer (EDS) and Synchronization Radiation X-ray diffractometer (XRD, energy: 20 keV, spot size: 3 μm×3 μm, angle of incidence: 0.5°). Additionally, JMatPro software was used to calculate the temperature-phase composition diagram and the element distribution during the homogenization process.

3 Results

3.1 Homogenization condition selection

The primary alloying elements in the GH3535 alloy originate from the transition metal d-zone, and these elements exhibit varying degrees of segregation. For example, chromium (Cr) tends to segregate positively in the interdendritic regions during solidification, and molybdenum (Mo) shows positive segregation in the dendritic arms. Conversely, iron (Fe) demonstrates negative segregation within the dendritic arms of initially solidified dendrites. The principle of thermodynamic homogenization obeys the element diffusion across different regions of the alloy, which is driven by chemical potential gradients. The chemical potential gradients facilitate movement from areas of higher chemical potential to those with lower chemical potential. The diffusion process during homogenization can be described by Fick ' s first law of diffusion, which is represented by a function for the diffusion coefficient, as follows:

$$D = D_0 e^{-Q/RT}$$

where D is the diffusion coefficient, Q is the diffusion activation energy, R is gas constant, T is the thermodynamic temperature, and D_0 is the diffusion constant independent of temperature. D_0 and Q vary with the composition and structure of the alloy, but they are often considered as constants. The diffusion coefficient D and temperature T follow an exponential relationship. High temperature increases atomic

energy, facilitating migration and resulting in a high diffusion coefficient and a fast diffusion rate, which accelerates uniform diffusion. Consequently, appropriately raising the homogenization temperature can enhance the homogenization efficiency. To prevent overheating of the alloy, it is generally recommended that the homogenization temperature should be set within $0.90T_m$–$0.95T_m$, where T_m represents the actual melting temperature of the casting. Fig. 2 illustrates both heating and cooling curves obtained from DTA for the GH3535-Y alloy. During heating, peak temperatures corresponding to the endothermic peaks within 1200–1450 °C are recorded at 1268, 1409, and 1418 °C. Additionally, the start temperature for the endothermic peak is between 1300 – 1410 ° C, and it is approximately estimated as 1387 ° C. Upon cooling, an exothermic peak can be observed at 1289 ° C with an extrapolated start point at around 1292 °C. Similarly, another exothermic peak occurs at 1166 °C. However, as depicted in Fig. 3, when the temperature exceeds 1000 °C, the proportion of M_6C phase in the alloy is decreased with the increase in temperature (Fig. 3b). Considering the potential measurement deviation, the final homogenization temperatures are determined as 1150 and 1188 °C. Furthermore, based on the microstructure observations of alloys after homogenization for different durations (2, 5, and 10 h), the influence of homogenization time on the alloy structure was investigated.

3.2 Microstructure before and after homogenization

Fig.4 illustrates OM morphologies of GH3535-0.08Y alloys before (as-cast) and after homogenization under different conditions. The as-cast structure displays a pronounced dendritic pattern, which is characterized by elongated coarse grains. After homogenization at 1150 °C for 10 h (Fig.4d), the dendritic structure within the alloy is eliminated. There are some dispersed black spots, which are suspected as precipitated phases. Both the quantity and size of the black spots in the as-cast alloy are decreased with the prolongation of homogenization time. However, after homogenization at 1188 °C for 10 h (Fig. 4g), the dendrites cannot be observed, and the black spot size is increased, accompanied by the emergence of a schistose structure. Metallographic etching may influence the observation of the alloy precipitates. Therefore, direct OM observation (without metallographic etching) was conducted on the polished samples, as illustrated in Fig. 5. All homogenization samples exhibit distinct and uniformly distributed black spots. In comparison to that of the as-cast sample, the quantity of black spots in the homogenization samples significantly decreases. The sample subjected to homogenization at 1150 °C for 10 h exhibits the smallest number of black spots. Conversely, for the sample after homogenization at 1188 ° C for 10 h, a markedly larger number of black spots can be observed.

Fig. 6 shows SEM microstructures of GH3535-0.08Y alloys before and after homogenization under different conditions. The black spots within the alloy are precipitated phases. Their chemical composition is detailed in Table 2. Fig.7 shows SEM images and corresponding EDS element mappings of precipitated phases in GH3535-0.08Y alloys before and after homogenization under different conditions. XRD patterns of GH3535-0.08Y alloys before and after homogenization under

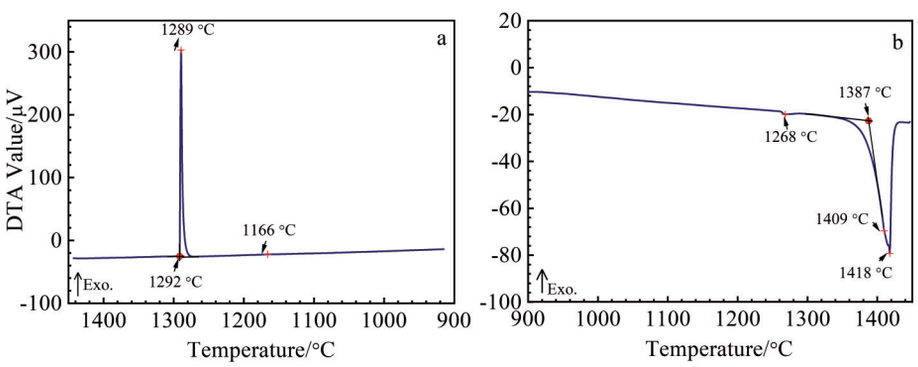

Fig.2 DTA curves of as-cast GH3535-0.08Y alloy: (a) cooling curve and (b) heating curve

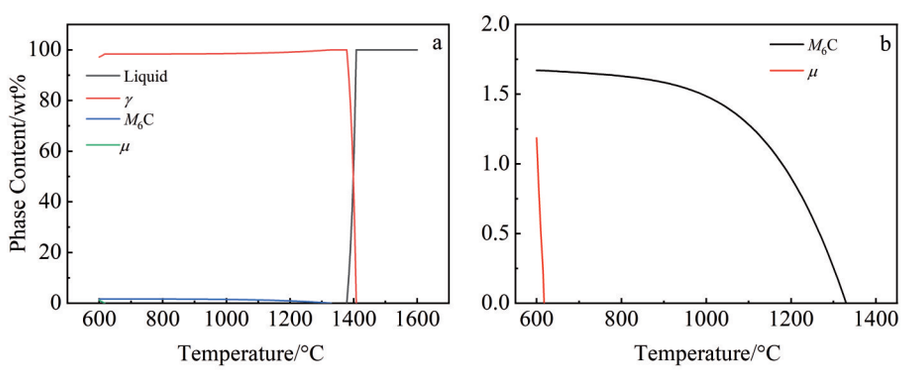

Fig.3 Phase contents calculated by JMatPro software: (a) overall; (b) precipitated phases

Fig.4 OM morphologies of GH3535-0.08Y alloys with metallographic etching before (a) and after homogenization at 1150 °C (b–d) and 1188 °C (e–g) for 2 h (b, e), 5 h (c, f), and 10 h (d, g)

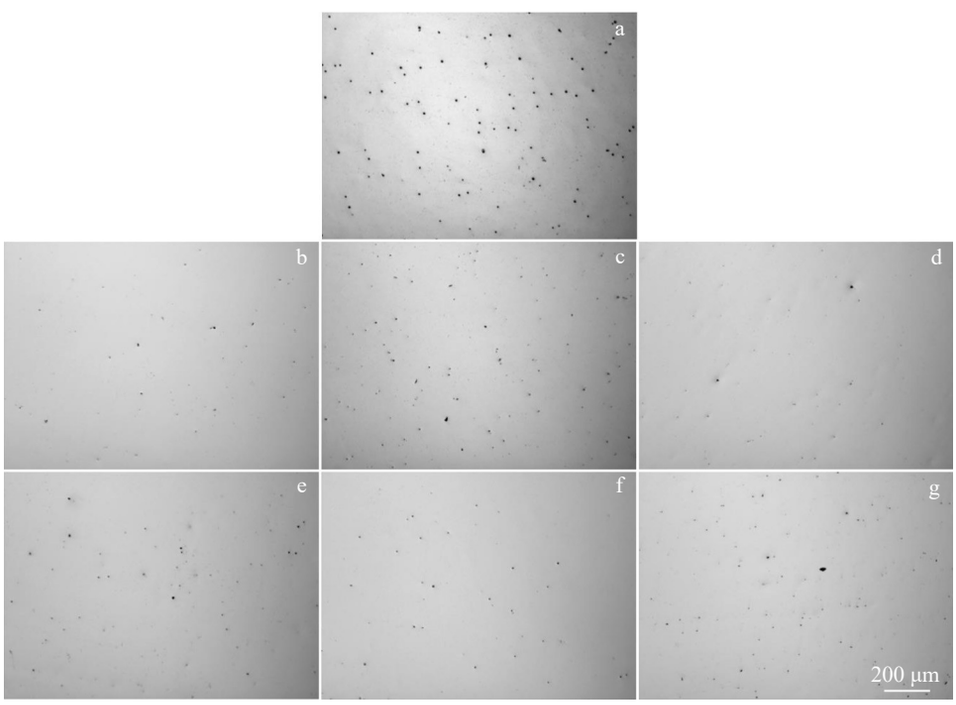

Fig.5 OM microstructures of GH3535-0.08Y alloys without metallographic etching before (a) and after homogenization at 1150 °C (b–d) and 1188 °C (e–g) for 2 h (b, e), 5 h (c, f), and 10 h (d, g)

different conditions are presented in Fig.8. In the as-cast alloy, three primary types of phases are identified: SiC, Y_2O_3, and Y_5Si_3. For the samples after homogenization at 1150 and 1188 °C for 2–10 h, the content of SiC and Y_5Si_3 shows a significant decreasing trend. The morphology of SiC does not change significantly, still presenting a hill-like protrusion. However, the edges of Y_5Si_3 gradually become indistinct due to internal decomposition processes. Besides, the decrease in Y_5Si_3 content is more significant at 1188 °C than at 1150 °C. Conversely, for the sample subjected to homogenization at 1188 °C for 10 h, there is also a notable decrease in SiC content. However, some overburnt holes appear[17–20], as shown

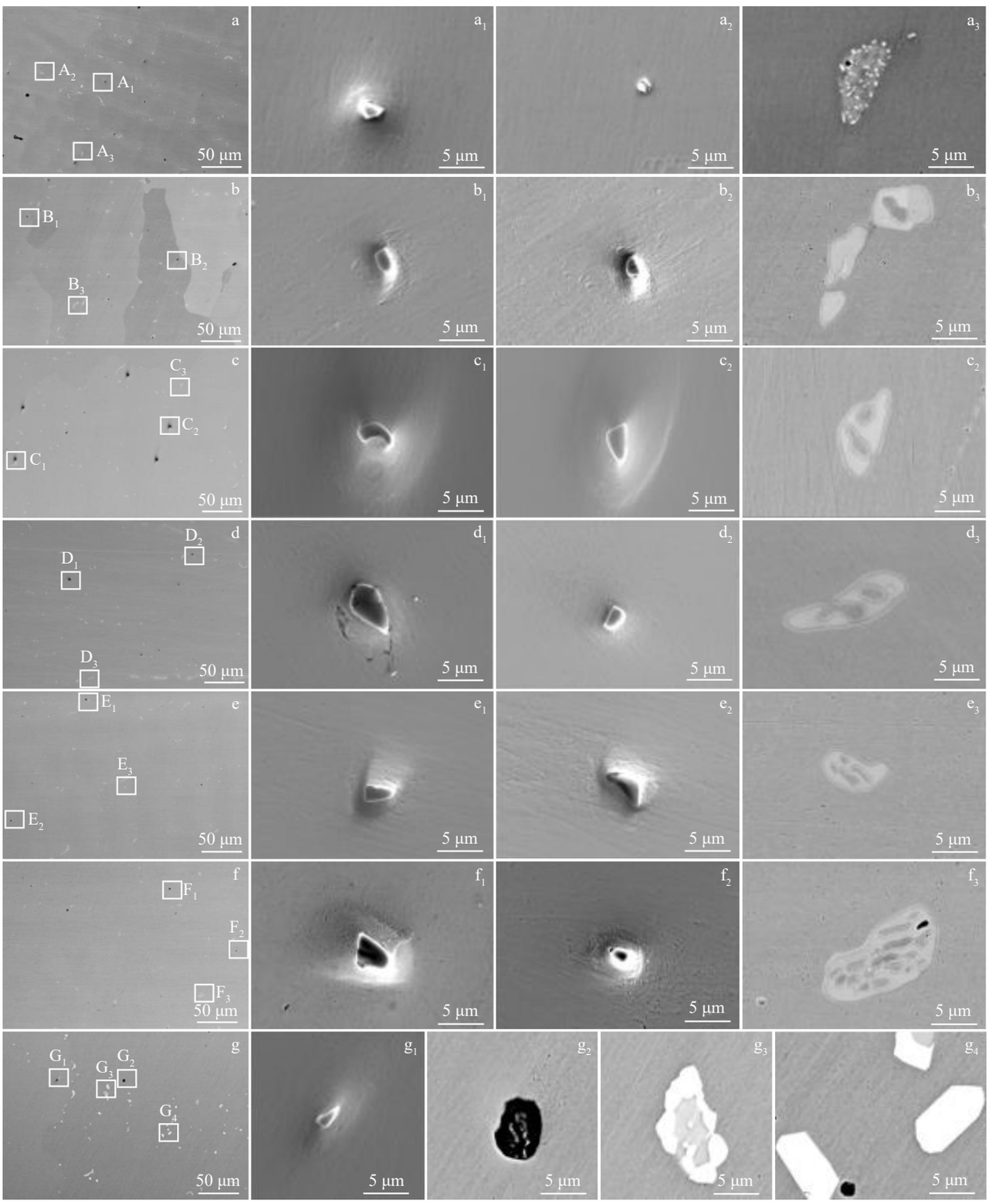

Fig.6 SEM microstructures of GH3535-0.08Y alloys before (a) and after homogenization at 1150 °C (b–d) and 1188 °C (e–g) for 2 h (b, e), 5 h (c, f), and 10 h (d, g); magnified images of area A_1 (a_1), area A_2 (a_2), and area A_3 (a_3) in Fig.6a; magnified images of area B_1 (b_1), area B_2 (b_2), and area B_3 (b_3) in Fig.6b; magnified images of area C_1 (c_1), area C_2 (c_2), and area C_3 (c_3) in Fig.6c; magnified images of area D_1 (d_1), area D_2 (d_2), and area D_3 (d_3) in Fig.6d; magnified images of area E_1 (e_1), area E_2 (e_2), and area E_3 (e_3) in Fig.6e; magnified images of area F_1 (f_1), area F_2 (f_2), and area F_3 (f_3) in Fig.6f; magnified images of area G_1 (g_1), area G_2 (g_2), area G_3 (g_3), and area G_4 (g_4) in Fig.6g

in Fig. 6g_2, along with new precipitates around the Y_5Si_3 particle. These new precipitates (Fig.6g_3–6g_4) are enriched in Mo and Si, except Y. Fig.8c indicates the presence of the M_6C phase in the GH3535-0.08Y alloy after homogenization at

1188 °C for 10 h. Based on the atomic ratio of M_6C in Table 3[17,21], it can be deduced that these precipitates are M_6C phase, which constitutes the primary precipitates in GH3535 alloy[22–24]. Under this homogenization condition, Y_5Si_3 gradually decomposes, the Si in Y_5Si_3 is combined with Mo surrounding Y_5Si_3 to form M_6C, the Y content in Y_5Si_3 gradually decreases, and finally, the number of Y_5Si_3 decreases significantly, as indicated by Fig.$6g_3$–$6g_4$. The results in Table 2 can also support this conclusion. In Fig. $6g_3$, the Y_5Si_3 is surrounded by the M_6C phase, and the content of Si in Y_5Si_3 is lower than that in M_6C. It is also found that Mo tends to be enriched around the Y precipitates[9]. In Fig.$6g_4$, the M_6C forms completely with only a little bit of Y around the edges of M_6C phase, which indicates that the enriched Y in this part diffuses into the matrix. While M_6C serves as a principal precipitation strengthening phase within the Hastelloy alloy, an excessive presence of large-sized M_6C during homogenization is undesirable[25–26].

3.3 Element distribution before and after homogenization

Fig. 9 shows the microstructure and EPMA element distribution analyses of GH3535-0.08Y alloy before homogenization. The microstructure exhibits a pronounced dendritic structure, Mo exhibits a significant positive segregation in the dendrite cores, whereas Ni and Cr display a moderate degree of positive segregation between the dendrites. The dendritic structure progressively diminishes after homogenization treatments at 1150 and 1188 °C for 2–10 h. For the samples subjected to homogenization at 1150 and 1188 °C for 10 h, the dendrites are eliminated (Fig. 4). EPMA analysis of the sample homogenized at 1150 °C for 10 h (Fig. 10) indicates that original element segregation is eliminated. Using JMatPro software, with an average secondary dendrite arm spacing of 31.3 μm of the as-cast sample, it is possible to calculate the distribution of the major segregation-prone elements (Cr, Mo, and Si) during various homogenization processes, as depicted in Fig.11. In the as-cast sample, the degree of segregation of Si, Cr, and Mo is serious; the contents of these elements in the dendrite regions are different. In addition, the degree of segregation of Si is slight. According to the JMatPro calculation results, after homogenization at 1150 °C for 2 h, the segregation of Si is eliminated (Fig. 11a). After homogenization at 1150 and 1188 °C for 10 h, separately, the segregation of Si, Cr, and Mo can be eliminated, and the elements are distributed uniformly (Fig. 11a, $11b_2$, and $11c_2$). The results demonstrate that homogenization can effectively modify element segregation within the as-cast sample, achieving optimal uniformity in element distribution after treatment at both temperatures for 10 h. Notably, actual measurements of dendritic segregation are closely aligned with the calculations performed using JMatPro software.

Table 2 Composition of areas marked in Fig.6 (wt%)

Area	C	O	Si	Cr	Y	Mo	Ni
Fig.6a (overall)	6.1	0.4	0.5	6.4	<0.1	17.4	69.3
A_1	25.3	0.6	56.3	1.6	0.9	4.0	11.3
A_2	6.6	14.3	0.4	3.2	33.0	11.5	31.1
A_3	8.6	0.4	1.1	4.4	9.2	27.2	49.2
Fig.6b (overall)	3.7	0.3	1.8	5.8	<0.1	16.6	72.1
B_1	19.4	1.0	39.6	3.4	<0.1	7.7	29.0
B_2	27.0	1.1	56.4	1.4	0.6	2.5	11.0
B_3	5.5	1.1	1.5	0.9	20.3	1.0	69.7
Fig.6c (overall)	6.8	0.5	0.4	6.5	<0.1	16.8	69.1
C_1	32.6	0.6	47.4	1.6	0.4	4.5	12.8
C_2	41.7	0.3	52.3	0.5	1.1	1.1	3.1
C_3	5.4	0.8	1.6	1.0	20.9	0.8	69.5
Fig.6d (overall)	6.2	0.3	0.4	6.6	<0.1	17.2	69.3
D_1	38.3	0.5	58.2	0.1	1.4	<0.1	1.6
D_2	32.0	5.5	17.6	3.4	0.2	8.0	33.4
D_3	5.5	1.1	1.5	0.9	20.3	0.9	69.9
Fig.6e (overall)	3.6	0.6	0.4	6.9	<0.1	16.0	72.5
E_1	9.2	0.2	80.2	1.3	0.0	2.6	6.6
E_2	22.0	<0.1	36.7	3.7	0.0	8.0	30.0
E_3	4.9	0.9	1.7	0.9	20.3	1.1	70.3
Fig.6f (overall)	4.0	0.4	0.3	6.9	<0.1	15.4	72.3
F_1	17.8	<0.1	39.1	3.7	<0.1	8.1	31.3
F_2	15.5	5.5	47.6	1.8	<0.1	6.7	23.4
F_3	4.8	0.6	1.6	1.0	20.5	1.1	70.4
Fig.6g (overall)	6.3	0.4	0.4	6.4	0.1	16.3	70.2
G_1	33.8	1.0	42.8	2.0	0.7	5.9	13.8
G_2	10.1	0.6	1.9	4.2	<0.1	55.7	27.4
G_3	5.4	0.6	1.0	0.1	19.4	1.6	71.1
G_4	9.0	<0.1	2.0	4.5	0.0	56.5	28.0

4 Discussion

The dendrite structure and element segregation of Y-modified GH3535 alloy are obvious in the as-cast alloy (Fig. 4). The solidification of the alloy solution is initiated at the inner wall of the crystallization and extends into the interior of the alloy liquid along a direction perpendicular to the cooling surface, resulting in a distinctly directional casting structure. As the solidification layer thickens, the heat transfer coefficient decreases, and the formation and inconsistent growth of inner and outer crystal nuclei lead to alterations in grain shape, orientation, and size. The segregation phenomenon induced by metal composition during solidification exacerbates the concentration gradients of Mo and other elements around grain boundaries as well as within crystallites (Fig. 8), thereby broadening the recrystallization temperature range and reducing nucleation rates, which ultimately results in coarse grains, as shown in Fig. 1. Local microstructure observations reveal that these internal structures of coarse grains exhibit a tree-like dendritic pattern, which is a common characteristic in metallic alloys after solidification.

GH3535 alloy is a nickel-based superalloy, which is strengthened through solid solution strengthening mechanisms. This process involves the incorporation of various metal elements into the alloy matrix as solute atoms, which induce

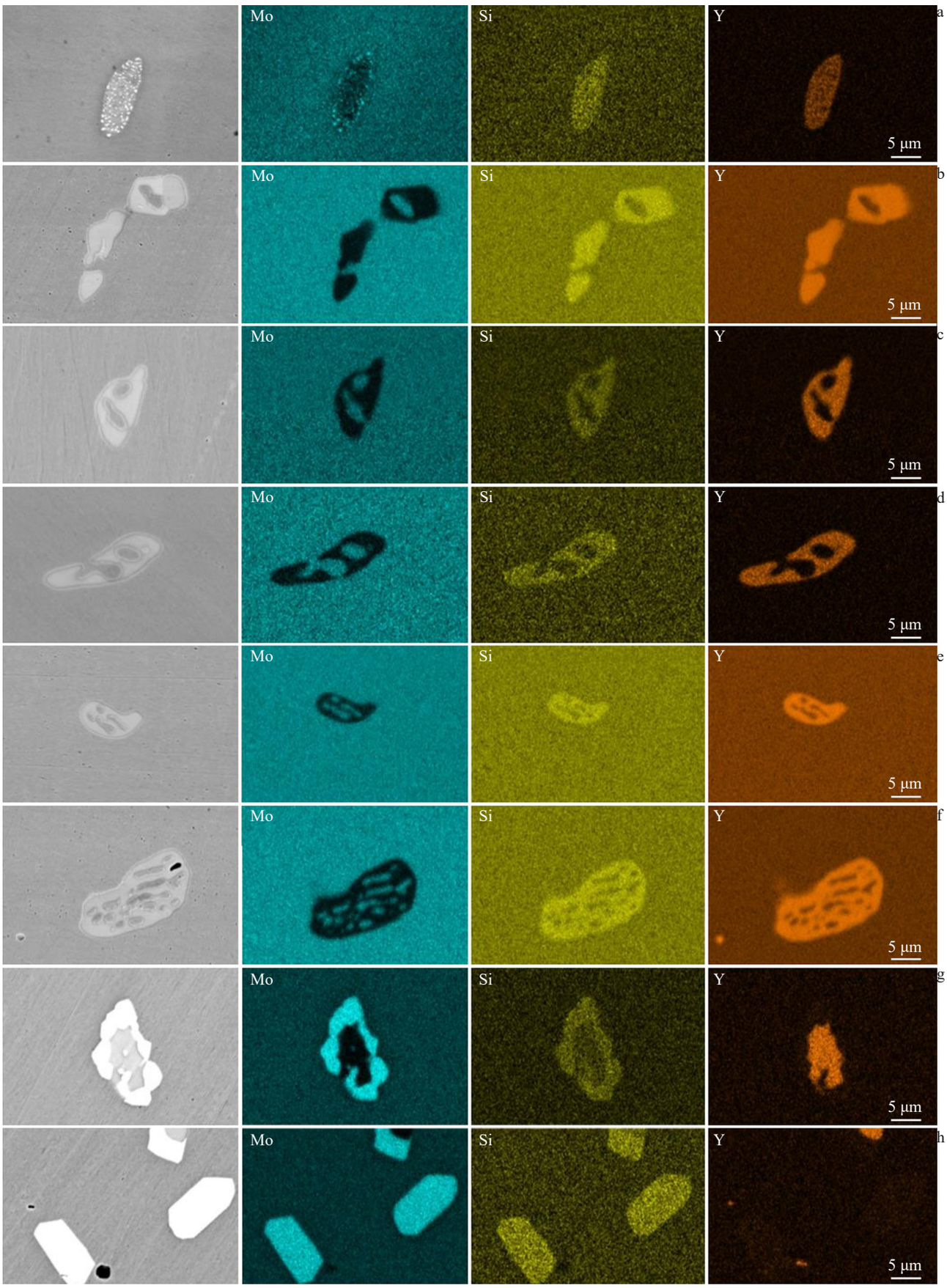

Fig.7 SEM images and corresponding EDS element mappings of precipitated phases in GH3535-0.08Y alloys before (a) and after homogenization at 1150 °C (b–d) and 1188 °C (e–h) for 2 h (b, e), 5 h (c, f), and 10 h (d, g–h)

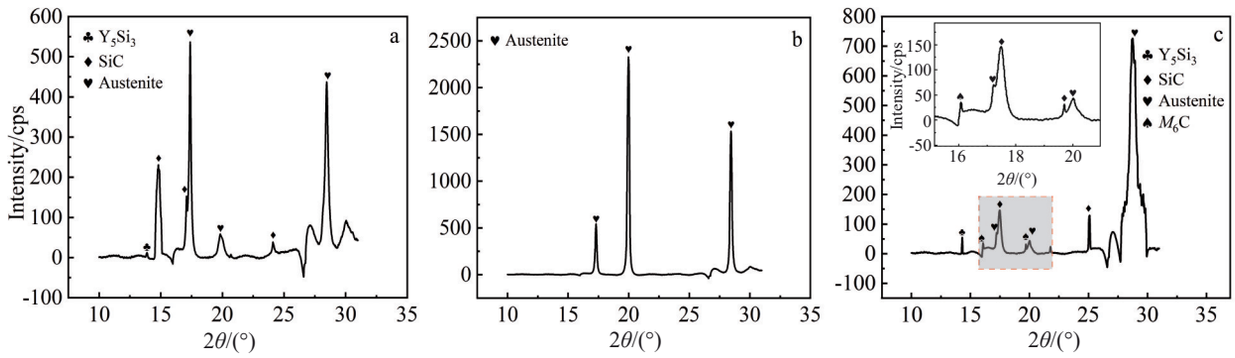

Fig.8 XRD patterns of precipitated phases in GH3535-0.08Y alloys before (a) and after homogenization at 1150 °C (b) and 1188 °C (c) for 10 h

Table 3 Empirical formulae based on atomic ratio of elements for carbide determination

Empirical formula	Type of carbide
Cr/(Cr+Mo+0.7W)<0.72	M_6C
Cr/(Cr+Mo+0.7W)>0.82	$M_{23}C_6$
0.72≤Cr/(Cr+Mo+0.7W)≤0.82	Change with heat treatment

local lattice distortions and impede dislocation movement, thereby enhancing the hardness and strength of the alloy. Typically, high-melting-point elements with suitable solubility and significant size effects are effective in reinforcing the alloy. The solute atoms in Y-modified GH3535 alloy are mainly Mo, Cr, and Y, all of which exhibit tendencies for segregation[27–30]. Among these elements, Mo serves as the principal solid solution strengthening element, and its melting point is 2620 °C. During solidification, Mo tends to segregate positively within the dendrites owning to its preferential crystallization behavior, while low-melting-point elements, such as Ni (melting point of 1457 °C), Cr (melting point of 1907 °C), and Y (melting point of 1522 °C), tend to segregate positively in interdendritic regions (Fig.9). Additionally, Y has

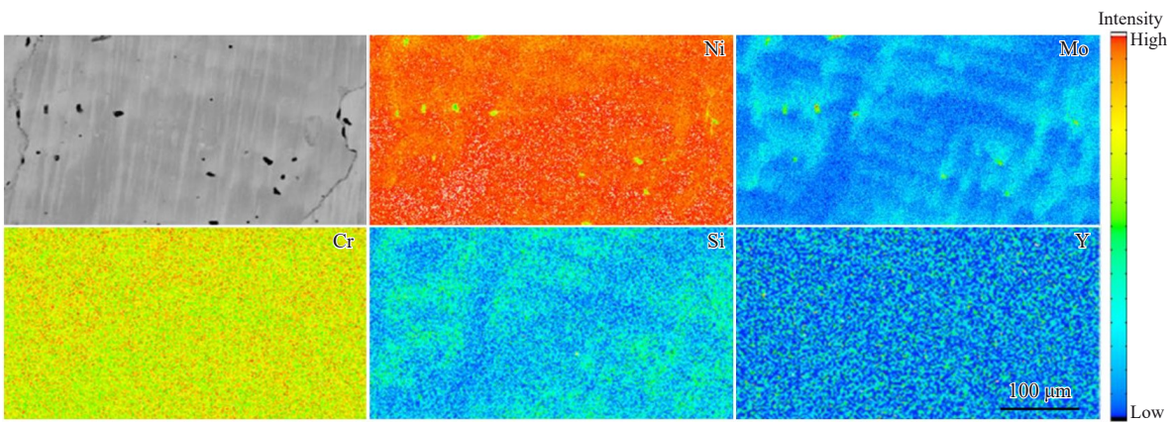

Fig.9 Microstructure and EPMA element distribution analyses of GH3535-0.08Y alloy before homogenization

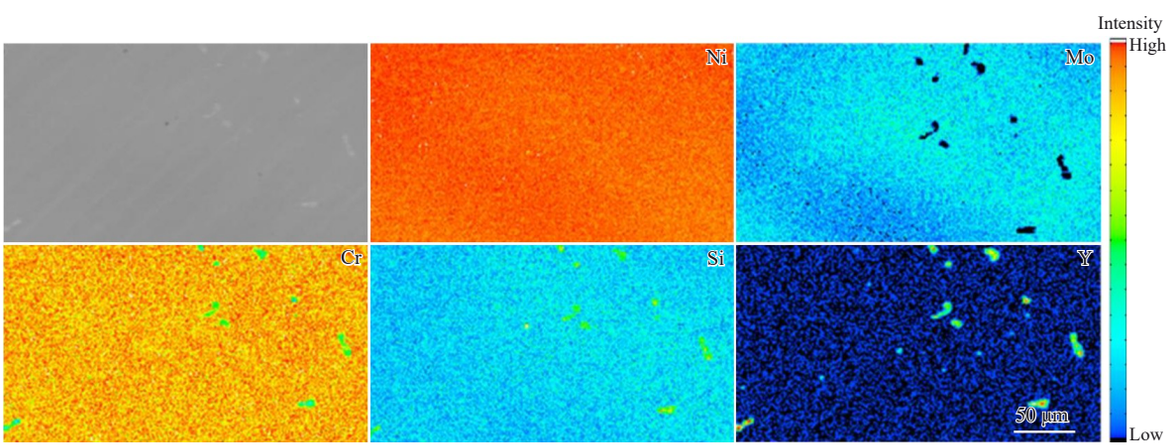

Fig.10 Microstructure and EPMA element distribution analyses of GH3535-0.08Y alloy after homogenization at 1150 °C for 10 h

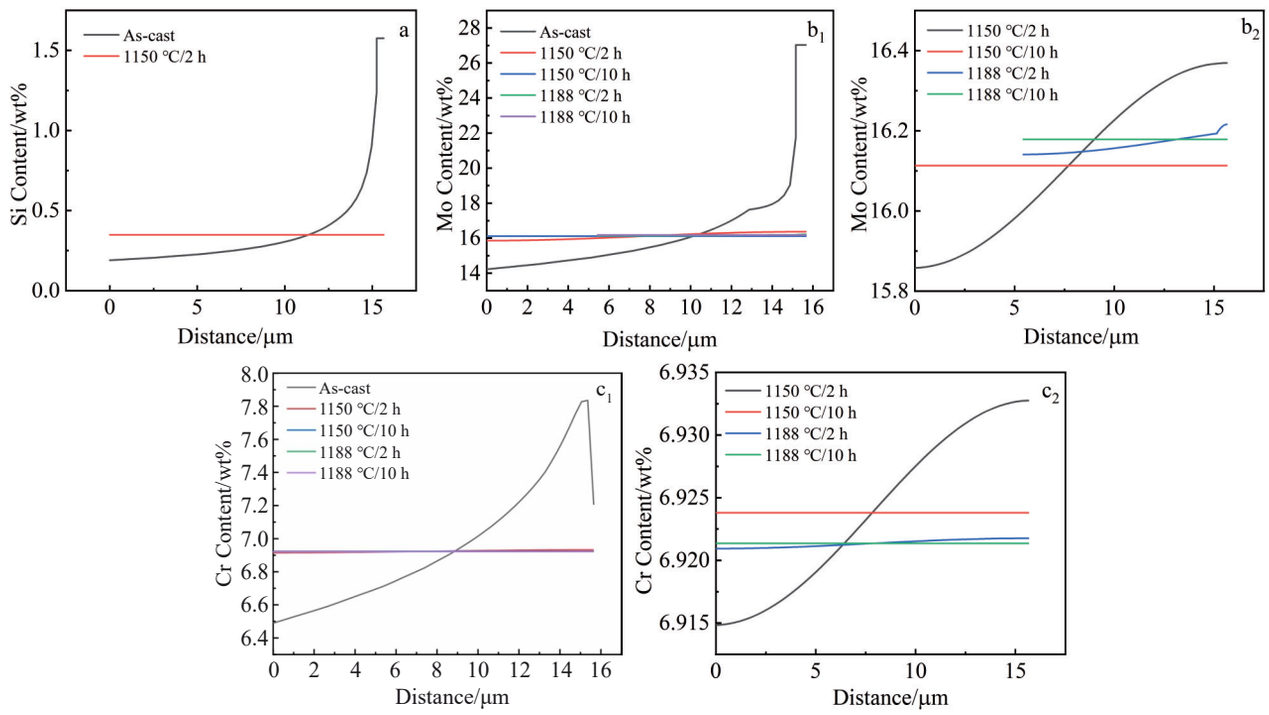

Fig.11 Element distributions between dendrites of GH3535-0.08Y alloys before and after homogenization: (a) Si; (b_1–b_2) Mo; (c_1–c_2) Cr

a large atomic radius and a large electronegativity difference with Ni/Cr atoms. Therefore, intermetallic compounds will form near the grain boundaries and interdendritic regions. The doping of Y decreases the initial melting point of nickel-based superalloy, which thereby affects the heat treatment temperature of the alloy and results in insufficient segregation elimination of Mo/Cr. Such micro-segregation within the alloy dendrites, particularly within the secondary dendrite arm spacing range, adversely affects the mechanical properties. Generally, smaller secondary dendrite arm spacing coupled with denser arrangement results in reduced element segregation within the alloy[28]. In the as-cast GH3535 alloy, this spacing is relatively small of 31.3 μm. With the prolongation of homogenization time to 10 h, the dendrites gradually diminish and ultimately disappear (Fig. 4). Concurrently, element segregation within the alloy is effectively eliminated (Fig. 9 – Fig. 10). However, homogenization at 1188 °C for 10 h results in a significant increase in defects within the alloy matrix (Fig. 6), potentially disrupting the continuity and adversely impacting the mechanical properties. This phenomenon suggests that 1188 °C exceeds the melting point of the low-melting phase in the alloy. Therefore, based on the structure assessments in this study, it can be concluded that the optimal homogenization condition for GH3535 alloy is 1150 °C/10 h.

Furthermore, significant phase transformations occur in the precipitated phase of the alloy during the homogenization process. Before homogenization, the as-cast alloy predominantly contains three phases: SiC, Y_5Si_3, and a minimal amount of Y_2O_3 (Fig. 6). With the prolongation of homogenization at 1188 °C from 2 h to 10 h, SiC gradually decreases in size and then almost disappears. At this temperature, the Gibbs free energy of the SiC formation (Si+C →SiC) is − 60 040.4 J indicating that it is not prone to decomposition during the homogenization. SEM analysis shows that some dispersed small-sized M_6C phases appear in the alloy after homogenization, Si and C are the main components of M_6C phase, and Si plays a stabilizing role in M_6C[24]. Therefore, it can be inferred that the disappearance of SiC can be mainly attributed to phase transformation. Additionally, the Y_5Si_3 phase also gradually decomposes. When the homogenization time is 2 and 5 h, the boundary between the phase and the alloy matrix gradually becomes blurred. When the homogenization time is 10 h, the outer rim is surrounded by M_6C phase, and many Y_5Si_3 phases already disappear, as shown in Fig. 7g–7h. When the homogenization temperature decreases to 1150 °C, the evolution of SiC is consistent with that at 1188 °C. At 1150 °C, the Gibbs free energy of SiC formation (Si+C→SiC) is − 60 354.2 J. SiC experiences the phase transformation rather than decomposition under this condition. During the homogenization from 2 h to 10 h, the edges of the Y_5Si_3 phase become more and more blurred, and the Mo-rich particles no longer exist within the Y_5Si_3 phase, compared with those in the as-cast alloy, resulting in more uniform element distribution (Fig. 7a – 7d). However, due to the lower temperature compared to 1188 °C, the Y_5Si_3 phase decomposes gradually in the alloy after homogenization at 1150 °C for 10 h, but significant phase changes cannot be observed. Furthermore, a little bit of Y_2O_3 produced during smelting cannot be detected after homogenization within specific areas.

Dispersed small-sized carbides can impede the dislocation

movement during high-temperature deformation, thereby enhancing the strength of the alloy. Micron-scale dispersed carbides can also inhibit the grain growth, therefore refining the grains of the alloy. However, the larger-sized carbides may induce stress concentration during the strain process, the carbide-matrix interfaces become the sites for crack nucleation, and subsequent crack is initiated, which is detrimental to the high-temperature mechanical properties of the alloy[21,31–33]. Additionally, during molten-salt corrosion, an electrochemical corrosion can occur between carbides and the matrix, weakening the resistance against the high-temperature molten-salt corrosion of the alloy[34]. Consequently, homogenization at 1188 °C is unsuitable for GH3535 alloy since both SiC and Y_5Si_3 phases are converted into larger carbides that generating M_6C particles of approximately 10 μm or larger in size.

Based on the abovementioned analyses of dendritic microstructure, element distribution, alloy defects, and precipitated phase evolution within the GH3535 alloy, it can be concluded that the homogenization treatment at 1150 °C for 10 h is optimal. Besides, after homogenization at 1150 °C for 10 h, the element segregation is eliminated and there are only a few dispersive precipitates in the Y-modified GH3535 alloy. This result brings great benefits to the subsequent forging and other heat treatment processes of the alloy, which can improve the high-temperature mechanical properties. Therefore, the Y-modified GH3535 alloy is expected to play an important role in the key structural components of molten salt reactors at higher operating temperatures in the future.

5 Conclusions

1) As-cast Y-modified GH3535 alloy exhibits elongated coarse grains characterized by a distinct dendritic structure with Mo, Si, Cr, and Y as the main segregating elements. Three precipitates are identified in the as-cast alloy: SiC, Y_5Si_3, and Y_2O_3.

2) The addition of 0.8wt% Y decreases the homogenization temperature of GH3535 alloy. After the homogenization at 1150 and 1188 °C for 10 h, the dendritic structure completely disappears, and element segregation is eliminated. However, at 1188 °C, over-burning holes emerge, which adversely affects the properties of GH3535 alloy. Consequently, homogenization at 1150 °C for 10 h is identified as the optimal homogenization condition.

3) The precipitated phases undergo significant changes during homogenization. At 1150 °C, both SiC and Y_5Si_3 are gradually decreased in size with the prolongation of homogenization time from 2 h to 10 h, and the Y_5Si_3 phase can be observed. The boundary of the Y_5Si_3 becomes increasingly indistinct, accompanied by internal elemental diffusion. Similarly, at 1188 °C, SiC and Y_5Si_3 also exhibit a gradual reduction trend with the prolongation of homogenization time from 2 h to 10 h. After homogenization at 1188 °C for 10 h, partial Y_5Si_3 decomposes, Y is diffused into the matrix uniformly, and the Si is combined with the precipitated Mo to form M_6C phase.

References

1 Jérôme S, Michel A, Ondřej B *et al*. *Progress in Nuclear Energy*[J], 2014, 77: 308

2 Zhou Xingtai, Li Zhijun, Lu Yanling *et al*. *Strategic Study of CAE*[J], 2019, 21: 29

3 Wang Man, Nai Qiliang, Qiu Jun *et al*. *CMC 2017: Advances in Energy and Environmental Materials*[C]. Singapore: Springer, 2018: 133

4 Wang Hang, Wang Aiqin, Li Changyi *et al*. *Reviews on Advanced Materials Science*[J], 2022, 61: 873

5 Rong Lirong, Wang Min, Xing Weiwei *et al*. *Journal of Materials Science & Technology*[J],2023, 159: 112

6 Li Qingling, Zhang Huarui, Cheng Ying *et al*. *Journal of Materials Research and Technology*[J], 2013, 26: 3353

7 Li Xiaoli, Leng Bin, Ye Xiangxi *et al*. *Corrosion Science*[J], 2022, 194: 109940

8 Li X L, He S M, Zhou X T *et al*. *Materials Characterization*[J], 2024, 95: 171

9 Zhu Zhenyuan, Han Fenfen, Jia Yanyan *et al*. *Corrosion Science*[J], 2023, 216: 111091

10 Wang Guowei, Huang Lan, Tan Liming *et al*. *Materials Science and Engineering A*[J], 2022, 859: 144188

11 Gong T Z, Chen Y, Li D Z *et al*. *Journal of Alloys and Compounds*[J], 2024, 1006: 176259

12 Paul D J, Christopher J C. *Metallurgical and Materials Transactions B*[J], 2009, 40: 182

13 Shi Xiao, Duan Shengchao, Yang Wensheng *et al*. *Metallurgical and Materials Transactions B*[J], 2018, 49: 1883

14 Li Xinxu, Jia Chonglin, Zhang Yong *et al*. *Vacuum*[J], 2020, 177: 109379

15 Seyed A H, Karim Z M, Seyed M A. *Materials Science and Engineering A*[J], 2017, 689: 103

16 Zhou P J, Yu J J, Sun X F *et al*. *Scripta Materialia*[J], 2007, 57: 643

17 Huang Meiqian, Zhou Zijian, Cui Chuangyong *et al*. *Materials Characterization*[J], 2023, 204: 113211

18 Li S J, Peng K, Yang Y T *et al*. *2009 International Conference on Manufacturing Science and Engineering*[C]. Zhuhai: Trans Tech Publications, 2010: 97

19 Zhang S X, Qu S M. *3rd International Conference on Manufacturing Science and Engineering*[C]. Xiamen: Trans Tech Publications, 2012: 476

20 Zhang Shuang, Wang Hongxia. *Heat Treatment of Metals*[J], 2011, 36(12): 34 (in Chinese)

21 Chen Shuangjian, Ye Xiangxi, Yu Kun *et al*. *Materials Science and Engineering A*[J], 2017, 682: 168

22 Jiang Li, Ye Xiangxi, Liu Renduo *et al*. *Materials Letters*[J], 2019, 250: 167

23 Jiang Li, Zhang Wenzhu, Xu Zhoufeng *et al*. *Materials & Design*[J], 2016, 112: 300

24 Jiang Li, Ye Xiangxi, Wang Zhiqiang *et al*. *Journal of Alloys and Compounds*[J], 2017, 728: 917
25 Song Xiaoqing, Wang Yongxin, Gong Junjie *et al*. *Materials Characterization*[J], 2023, 196: 112640
26 Buerstmayr R, Theska F, Webster R *et al*. *Materials Characterization*[J], 2021, 178: 111250
27 Li J G, Wang N, Liu J D *et al*. *Journal of Materials Science & Technology*[J], 2024, 195: 9
28 Jia Lei, Cui Heng, Yang Shufeng *et al*. *Materials Characterization*[J], 2024, 209: 113735
29 Zhao Xiaoxiao, Wang Yongxin, Song Xiaoqing *et al*. *Computational Materials Science*[J], 2022, 202: 110990
30 Martin D, Pei Z R, Kyle R *et al*. *Materialia*[J], 2020, 13: 100843
31 Chen S J, Tsang D K L, Jiang L *et al*. *Materials Science and Engineering A*[J], 2017, 699: 48
32 Hu Rui, Bai Guang, Li Jinshan *et al*. *Materials Science and Engineering A*[J], 2012, 548: 83
33 Jiao S Y, Zhang M C, Zheng L *et al*. *Metallurgical and Materials Transactions A*[J], 2010, 41: 26
34 Danon A E, Muránsky O, Karatchevtseva I *et al*. *Corrosion Science*[J], 2020, 164: 108306

均匀化对钇改性GH3535合金微观组织特征的影响

王雨苗[1,2]，梁文君[2,3]，李晓丽[2]，蒋　升[4]，周兴泰[2]，邱汉迅[1]
(1. 上海理工大学 材料与化学学院，上海 200093)
(2. 中国科学院 上海应用物理研究所，上海 201800)
(3. 中国科学院大学 核科学与技术学院，北京 100049)
(4. 中国科学院 上海高等研究院，上海 201210)

摘　要：研究了均匀化参数对GH3535-0.08wt% Y合金中元素偏析、枝晶组织和析出相演变的影响。此外，在整个实验过程中，特定的均匀化参数保持不变。结果表明，在1150 ℃下加热10 h是最佳的均匀化条件。在这种条件均匀化处理后，枝晶结构和元素偏析被完全消除。铸态合金中存在的SiC和Y_5Si_3相均显著减少。然而，在1188 ℃时进行均匀化会导致合金内部出现过热缺陷；尽管SiC和Y_5Si_3也减少，但观察到一些较大的M_6C相，这会对后续的锻造工艺产生不利影响。

关键词：镍基合金；钇；微观组织；均匀化；碳化物

作者简介：王雨苗，女，2000年生，硕士生，上海理工大学材料与化学学院，上海 200093，E-mail：wangyumiao@sinap.ac.cn